Inner Bremsstrahlung in Muon Decay*

CHARLES A. REY†
The Enrico Fermi Institute for Nuclear Studies and Department of Physics, The University of Chicago, Chicago, Illinois

(Received 16 March 1964)

A measurement of inner bremsstrahlung in muon decay has been made using spark chambers, scintillators and fast oscilloscopes. The electron range distribution in graphite and the absolute rates were determined for electron–gamma-ray angles between 130 and 180 deg. For the electron and gamma-ray energies studied, the branching ratio of $\mu \rightarrow e+\gamma+\nu+\bar{\nu}$ to $\mu \rightarrow e+\nu+\bar{\nu}$ is predicted to be about 10^{-4} over this angular range. The total number of inner bremsstrahlung events observed was 1805 ± 43, which is in agreement with an expected number of 1889 ± 283. The data were found to be in accord with the predictions given by electromagnetic corrections applied to the weak interaction.

I. INTRODUCTION

THE process $\mu \rightarrow e+\gamma+\nu+\bar{\nu}$ is the only case of a radiative decay of a lepton which is not complicated by strong couplings. It can be described in detail by taking into account the well-known electromagnetic terms in addition to weak interaction theory.[1–3] In particular, the calculations by Fronsdal and Überall and by Eckstein and Pratt give the differential ratio of $\mu \rightarrow e+\gamma+\nu+\bar{\nu}$ to $\mu \rightarrow e+\nu+\bar{\nu}$ as a function of the electron energy, gamma-ray energy, and the angle between the electron and gamma ray. Since the dominant terms result from the coupling of the electron current to the electromagnetic field, the inner bremsstrahlung process is not unlike the external bremsstrahlung of an electron. The over-all features are relatively insensitive to the exact form of the weak decay interaction and depend primarily on the electromagnetic interaction and the kinematics of the decay.

There are, therefore, definite predictions about the electron energy spectrum and the electron–gamma-ray angular distribution as well as the over-all rates which are readily subject to experimental verification. While the predominant emission of the gamma ray is in the same direction as the electron and modifies the Michel spectrum only slightly, the backward emission of the gamma ray has a marked effect on the energy of the electron. The present study deals with the electron energy spectrum in the backward direction as well as the predicted angular correlation between the electron and gamma ray. This measurement serves to test the theory of electromagnetic effects on weak decay processes.

Although the radiative decay has been observed by several workers,[4–6] a careful study of the angular dependence was not undertaken. The work of Kim, Kernan, and York was a study of the gamma-ray spectrum and decay rate in the forward direction. In three of the most recent works[6] the major object was the search for the $\mu \rightarrow e+\gamma$ decay, and the rate of the $\mu \rightarrow e+\gamma+\nu+\bar{\nu}$ decay in the region of 180° was studied in a limited manner.

The present experiment was also done simultaneously with a search for the decay $\mu \rightarrow e+\gamma$,[7] but special attention was devoted to $\mu \rightarrow e+\gamma+\nu+\bar{\nu}$. An array of spark chambers and scintillation counters was used to measure the branching ratio in the region of large angles between the electron and the gamma ray. Setting a minimum of 12 MeV on the energies of the electron and gamma ray, the total branching ratio is predicted to be about 10^{-4} for the angular range of 130–180 deg. The spark chamber provided the large solid-angle acceptance and good angular resolution which is required. The visual display of each event and the sharp time resolution between scintillation counter pulses served to identify the real events and to eliminate spurious backgrounds. Information about the electron energy spectrum was obtained by observing the range in graphite of each electron. This range distribution was then compared to the distribution calculated from the theoretical energy spectrum for the inner bremsstrahlung process.

II. EXPERIMENTAL SETUP

The spark chamber arrangement was designed to observe an electron and a gamma ray traveling in approximately opposite directions. The muons were allowed to decay at rest in a target in the center of the apparatus. On one side of the target a spark chamber and scintil-

* Research supported by the U. S. Office of Naval Research.

† A thesis submitted to the Department of Physics, The University of Chicago, in partial fulfillment of the requirements for the Ph.D. degree.

[1] A. Lenard, Phys. Rev. **90**, 968 (1953); T. Kinoshita and A. Sirlin, *ibid.* **107**, 593 (1957); N. Tzoar and A. Klein, Nuovo Cimento **8**, 482 (1958); R. H. Pratt, Phys. Rev. **111**, 649 (1958).

[2] C. Fronsdal and H. Überall, Phys. Rev. **113**, 654 (1959).

[3] S. G. Eckstein and R. H. Pratt, Ann. Phys. (N. Y.) **8**, 297 (1959).

[4] C. O. Kim, W. J. Kernan, and C. M. York, Phys. Rev. **120**, 983 (1960).

[5] J. Ashkin, T. Fazzini, G. Fidecaro, N. H. Lipman, A. W. Merrison, and H. Paul, Nuovo Cimento **14**, 1266 (1959); R. R. Crittenden, W. D. Walker, and J. Ballam, Phys. Rev. **121**, 1823 (1961).

[6] D. Bartlett, S. Devons, and A. M. Sachs, Phys. Rev. Letters **8**, 120 (1962); S. Frankel, J. Halpern, L. Holloway, W. Wales, M. Yearian, *et al.*, *ibid.* **8**, 123 (1962); S. Frankel, W. Frati, J. Halpern, L. Holloway, W. Wales, and O. Chamberlain, Nuovo Cimento **27**, 894 (1963).

[7] S. Parker, H. L. Anderson, and C. Rey, Phys. Rev. **133**, B768 (1964).

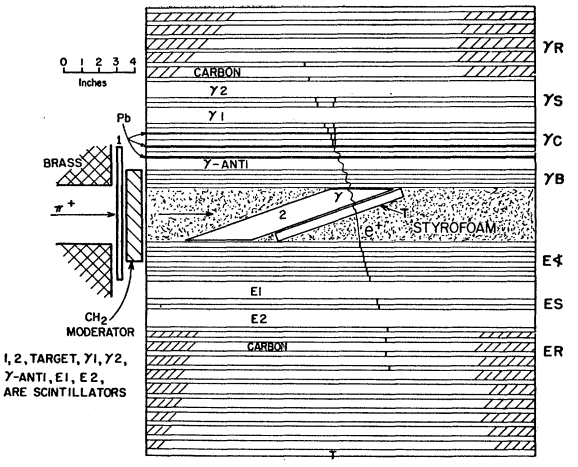

FIG. 1. Plan view of experimental setup.

lator assembly were used to detect the electron and to measure its direction and range in graphite. On the other side, the gamma ray was detected by a combination of lead plates, scintillators, and spark chambers.

A plan view of the experimental arrangement appears in Fig. 1. A π^+ beam of 65 MeV was taken from the University of Chicago synchrocyclotron. An internal vibrating target was used to obtain a smoothed time distribution of beam particles thus avoiding high instantaneous rates and high accidental rates. The pion beam was magnetically analyzed and passed through a two-foot-long lead and brass collimator. A plastic scintillator (1), which was $\frac{1}{4}$ in.$\times$8 in.$\times$8 in., completely covered the exit of the collimator. The pion beam entered next a polyethylene moderator, a scintillator (2), and the target scintillator (T). Both counter 2 and the target were slanted, with their normals at 70° to the beam. This allowed a thin target to present a large thickness to the beam direction. Hence, decay electrons could escape the target with a minimum of multiple Coulomb scattering, permitting an accurate determination of the electron-gamma angle. Counter 2, which provided moderation of the pion beam, was slanted so that it could be placed as close as possible to the target in order to minimize scattering losses.

A fraction (61%) of the pions that passed through the counter telescope (1, 2, T) stopped in the target and decayed to muons there. The electron side of the spark chamber consisted first of a section of eight gaps (E) to measure the direction of an electron from muon decay in the target. The electron was detected by two scintillators $E1$ and $E2$ (21 in.$\times$21 in.$\times\frac{3}{8}$ in.) separated by two gaps (ES) and $\frac{1}{2}$ in. of graphite. The electron's range was measured in a section of ten graphite plates, each followed by a spark chamber gap (ER). The graphite plates of density 1.66 gm/cc were $\frac{1}{2}$ in. thick except for the first, which was $\frac{1}{4}$ in.

The gamma side of the chamber consisted first of four gaps used as an antisection (γB), and a scintillator, $\bar{\gamma}$. This was followed by three conversion plates of 0.36 radiation length each. These plates were constructed of $\frac{1}{16}$-in. lead plates sandwiched between two stainless steel plates each 0.012 in. thick. These were pressed and glued together with Eastman "910" cement in order to provide a flat surface and to produce rigidity in the otherwise soft lead. Each conversion plate was followed by a double gap (γC). To detect the conversion electron there were two scintillators, $\gamma 1$ and $\gamma 2$, separated by a double gap (γS) and a $\frac{1}{4}$-in. graphite plate. This was followed by a range section of six graphite plates ($\frac{1}{2}$ in. thick), each followed by a single gap (γR). All spark chamber gaps were 21 in.$\times$21 in.$\times\frac{1}{4}$ in. and made with 0.012-in. aluminum plates.

Details of the modular gaps, the pulsing arrangement, and the gas and optical systems are given in a separate publication.[8]

A simplified block diagram of the electronics appears in Fig. 2. A pion was detected in the telescope by a (1, 2, T) coincidence. This was accepted only during the long spill of the beam (0.01 sec) and opened a gate $(1, 2, T)_G$ from 0.2 μsec to 11 μsec after the (1, 2, T). Moderately fast (15 nsec) coincidences were formed from the electron side ($E1$, $E2$, T) and from the gamma side ($\bar{2}$, $\bar{\gamma}$, $\gamma 1$, $\gamma 2$). The 2 pulse was placed in anticoincidence with the $\gamma 1$, $\gamma 2$, $\bar{\gamma}$ requirement in order to eliminate triggering on a muon which decays in 2. In this case, the electron would pass through more material than just the target, and thus would have larger errors in angle due to multiple Coulomb scattering. The output of the slow coincidence $(1, 2, T)_G(T, E1, E2)$ $(\bar{2}, \bar{\gamma}, \gamma 1, \gamma 2)$ then triggered the spark chamber and the oscilloscopes. Immediately after each trigger the electronics and scalers were blocked off for 2 sec to prevent the counting of noise from the spark chamber discharge and to give the cameras time to advance the film.

Three oscilloscope displays were photographed for each trigger of the spark chamber. Figure 3 shows a typical display. At the upper left, a 4-beam scope displayed the pulses from the scintillators $\gamma 2$, T, and $E2$, and a 100-Mc/sec sine wave for calibration. As each of these scintillators were seen by a pair of 56AVP phototubes, the anode pulses were added at the bases of these tubes, delayed and placed directly on the deflection plates of the 4-beam scope. The sweep speed was approximately 7 nsec per cm over most of the sweep. The times of the T, $E2$, and $\gamma 2$ pulses were then corrected for the light transit time in the scintillator using position data from the spark chamber pictures.[7] This precise timing was relied on to identify real events and to help eliminate accidental backgrounds.

Most accidentals were due to a genuine (T, $E1$, $E2$) event in accidental coincidence with a ($\bar{2}$, $\bar{\gamma}$, $\gamma 1$, $\gamma 2$) signal. By using a broad time resolution between these two signals in the electronics, both real and accidental events were counted permitting a simultaneous meas-

[8] C. Rey and S. Parker, Nucl. Instr. Methods **20**, 173 (1963).

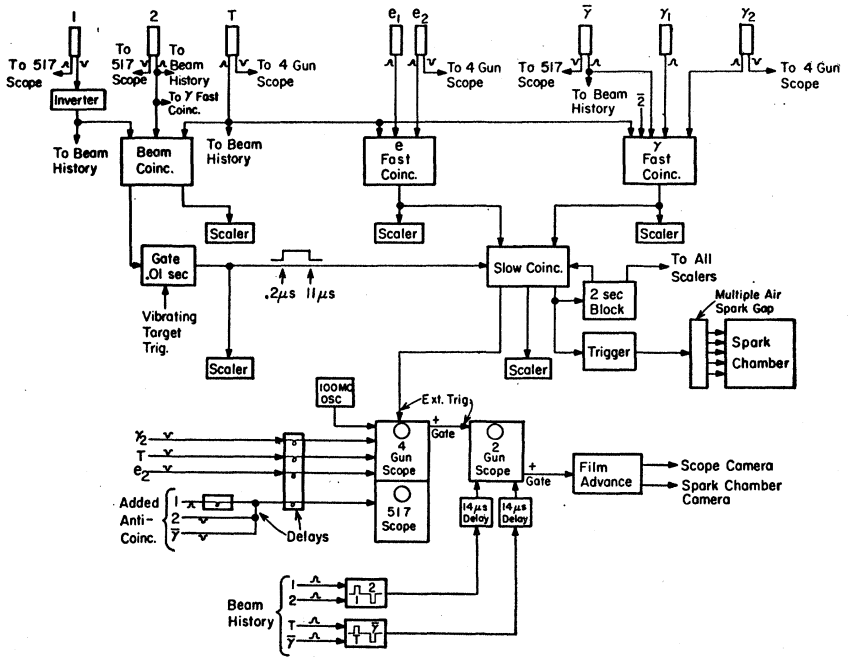

FIG. 2. Simplified electronics block diagram.

urement of the accidental rate. This cannot be done by scaling counts from an additional coincidence circuit with one input delayed, since only a small fraction of the out of time events produce acceptable spark chamber pictures.

Anode pulses from counters 2 and $\bar{\gamma}$, and a delayed positive dynode pulse from counter 1 were displayed on a single sweep of 20 nsec per cm on a 517 scope. The electronics rejected an event with a large 2 or $\bar{\gamma}$ prompt pulse with about 95% efficiency. The final rejection was set after the experiment by selecting a cutoff on the $(2, \bar{\gamma})$ pulse to give an anticoincidence efficiency as high as possible without losing triggering efficiency from afterpulsing or noise in counter 2.

Another scope, a dual beam Tektronix 551, with a sweep speed of 2 μsec/cm, provided a past history of the beam particles entering the spark chamber. Pulses from counters 1, 2, T, and $\bar{\gamma}$ each triggered a circuit which produced a shaped pulse of constant amplitude and width. Using Columbia HH-2000 delay cable the pulse from $2(-)$ was delayed 1.5 μsec and added to the 1 pulse $(+)$. This combination was delayed an additional 14 μsec and displayed on the upper trace of the 551. Pulses $T(+)$ and $\bar{\gamma}(-)$ were treated similarly, with $\bar{\gamma}$ 1.5 μsec later than T. These pulses were placed on the lower trace. Thus, the signature of a good event, shown in Fig. 3 was a 1, 2, T coincidence from the beam particle followed by a T pulse at prompt time.

The sweeps of the 2 fast scopes were finished before the arrival of interference produced by the spark chamber discharge. The pulses on the 551 scope were displayed on a portion of the sweep which occurred after interference had disappeared. The useful time on this trace was 10 μsec, with "prompt time" delayed to the 14-μsec point, thus avoiding the interference which appeared on the first 4 μsec of the trace.

III. ANALYSIS OF DATA

A total of 126 000 pictures were taken of the chamber and scopes. In order to eliminate most spurious and accidental events, the spark chamber pictures were scanned, with the following acceptance criteria:

(1) There should be only one electron track originating from the target and passing through the electron angle section to at least the $E2$ scintillator. Because of the high beam rate about 10% of the pictures showed 2 tracks on the electron side. These events were rejected.

(2) There must be a track originating from one of the lead converters passing to at least counter $\gamma 2$ with no track in the γB section pointing to the conversion point,

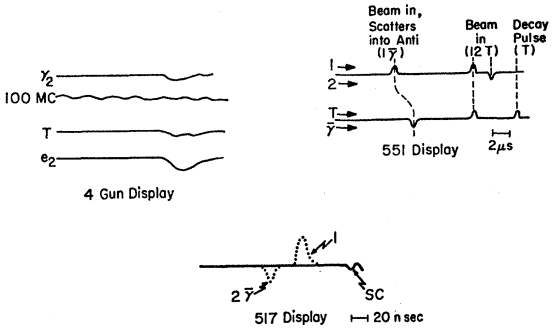

FIG. 3. Typical oscilloscope display. SC indicates the start of spark chamber interference on the 517.

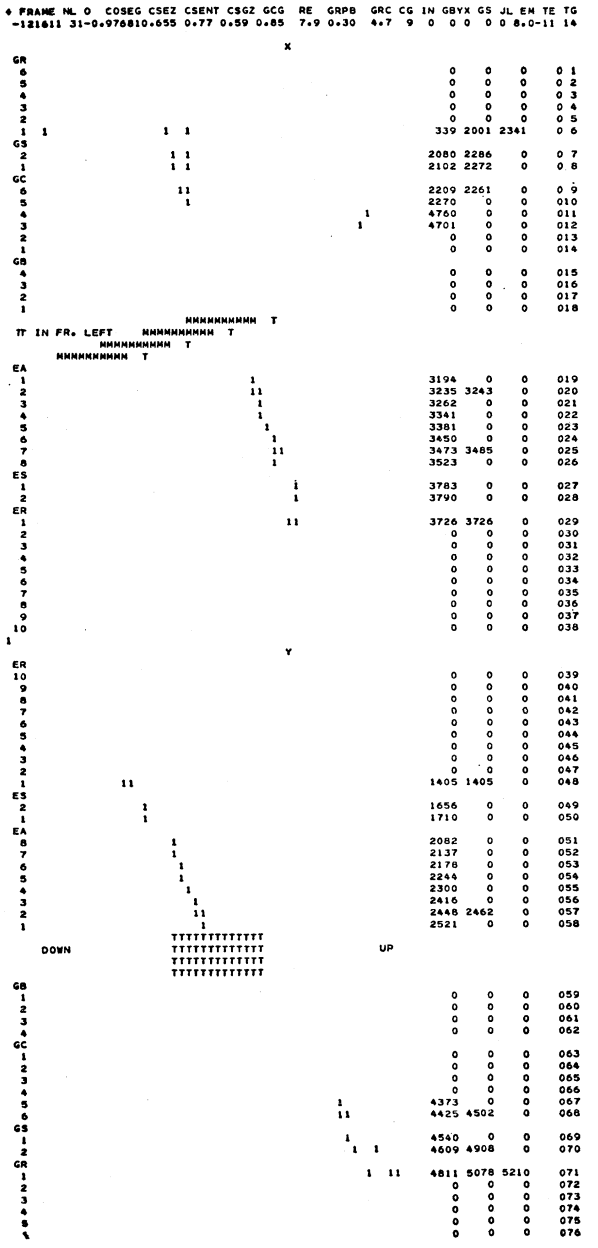

FIG. 4. A typical event reconstructed by the computer. For confusing or unusual events a final decision on spark and track selection could be made conveniently by hand.

and no track coming into the chamber from the front (beam side) and leading to the conversion point.

(3) There must be a prompt coincidence on the 4 beam scope between the $\gamma 2$, T, and $E2$ pulses. Hence, the $\gamma 2$, T, and $E2$ times must lie within 9 nsec of each other. This is a very liberal acceptance criterion chosen to insure 100% efficiency at this point in the data reduction.

(4) There must be no prompt 1 or $\bar{2}\bar{\gamma}$ pulse on the 517 trace.

(5) The data were divided into two groups with different criteria of acceptance on the estimated electron-gamma angle (θ). One group had wide limits, $120° \leq \theta \leq 180°$, and the other narrower ones, $150° \leq \theta \leq 180°$.

The remaining events, about 10 000 in number, were then measured more accurately on the measuring table of Hildebrand and Wright. By means of a computer, the electron direction was determined by a least-squares fit of a straight line to the spark positions in the electron angle section. This was projected back to the center of the target, and the gamma-ray direction determined from this point and the conversion point in lead. The ranges of the electron and the conversion electrons from the gamma ray were determined. The angles between the electron, gamma ray, and normal to the plates of the spark chamber were calculated. The computer program also calculated the timing corrections due to light transit times in the scintillators T, $E2$, and $\gamma 2$.

Many events, however, contained some sort of fault produced either by extra sparks in the chamber, by inefficiencies in the tracks of a good event, or by mistakes made at the measuring table. An extensive set of tests for such faults was made on each event by the computer and if an event failed these tests it was handled in a special manner. A code was punched indicating the type of fault and a sketch of the event was printed out showing pictorially and numerically all spark locations. Figure 4 shows a typical event reconstructed by the computer. These events were then examined by hand and coded corrections and instructions fed back to the computer which then reprocessed the event.

The errors in the measurement of the electron-gamma angle were ± 1.5 deg and the uncertainty due to multiple Coulomb scattering in the target was about 3 deg. These errors were not important in determining total rates since the branching ratio changes slowly as a function of angle.

Further selection criteria were applied to the results of these more accurate measurements. The angles ϕ_e and ϕ_γ of the electron and of the gamma ray with respect

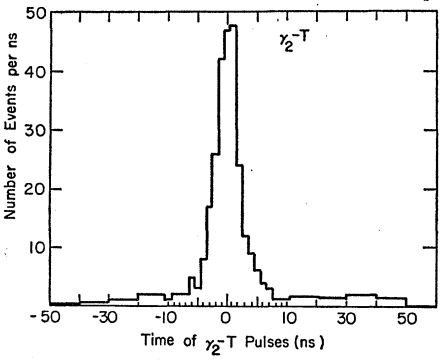

FIG. 5. Number of events as a function of the time difference between the $\gamma 2$ and T pulses (corrected for light collection time). Events outside the central 20 nsec are shown in 10 nsec groups on a compressed scale.

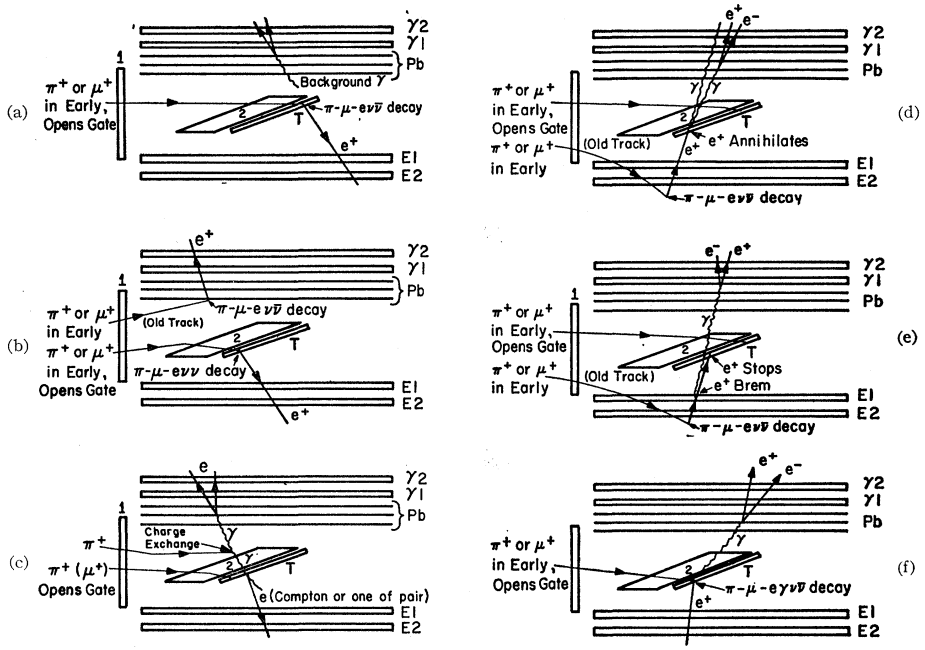

FIG. 6. Various events producing spark chamber triggers. (a) and (b): sources of time accidental backgrounds; (c), (d), and (e): sources of prompt backgrounds; (f): a typical event from $\mu \rightarrow e+\gamma+\nu+\bar{\nu}$.

to the normal of the chamber plates were limited to 50 and 45°, respectively, in order to obtain an easily calculable efficiency and solid angle. In addition, only events with θ between 180 and 125° were retained, as the detection efficiency falls off rapidly for smaller angles.

The angle between the gamma ray and the conversion electron with the greatest range was calculated, and if this angle was larger than 73° the event was eliminated. Background events caused by muons decaying in the lead planes do not have a correlation between the directions of the decay electron and the "gamma ray." At least 99% of all real events should have an angle between the electron and the gamma ray of less than 73°.

Further requirements on timing were applied after correcting the 4-beam scope times of $E2$, T, and $\gamma 2$ with the light transit time in the scintillator as determined by the spark chamber. This gives the timing curve in Fig. 5 with 50% points at ± 2 nsec and 95% points at ± 5 nsec. The accidental rate is given clearly by the wings of this curve. Timing cutoffs of ± 4 nsec were chosen to reduce the number of accidentals to 8% and yet maintain a moderately high efficiency (87%). After the application of the final selection criteria there remained about 2000 events. This number includes a small background contamination which was subtracted numerically.

IV. BACKGROUNDS

There are two basic categories of background. One is accidental, in which there is no time correlation between the gamma and electron sides, and the other is prompt or nonaccidental.

There are two sources of accidentals:

(1) A muon decays in the target by $\mu \rightarrow e+\nu+\bar{\nu}$ with the electron going into $E1$ and $E2$ and a gamma ray produced somewhere in the spark chamber or its vicinity converts in the lead plates and is detected in $\gamma 1$ and $\gamma 2$. See Fig. 6(a).

(2) A pion or muon in the beam scatters into the lead plates and the subsequent decay electron enters $\gamma 1$ and $\gamma 2$, in accidental coincidence with the $\mu \rightarrow e+\nu+\bar{\nu}$ as above. See Fig. 6(b).

Accidentals from these two sources were reduced to less than 8% by the fast timing and by restricting the angle between the conversion electron and the gamma ray. The second source is reduced further by rejecting events with a visible beam track going into the lead converters at or near the conversion point. The accidental rate is thus reduced to about 5%.

There are two kinds of prompt background:

(1) The beam gate is opened $(1, 2, T)_G$ by a pion, a second pion charge exchanges in the moderator or chamber walls, and the π^0 decays to a pair of gamma rays, with one gamma being detected in the gamma side and the other producing a pair or Compton electron in the target which goes into $E2$. See Fig. 6(c). This is eliminated with 100% efficiency by rejecting events with prompt 1's on the 517 trace. However, at the beginning of the run this pulse was not on the fast trace (the 517). This allowed a few background events of this type to go undetected in this part of the data. The fraction was estimated to be less than 2.5% of all the data.

(2) A pion scatters into $ES2$ or beyond and later the subsequent muon decays. The electron either annihilates

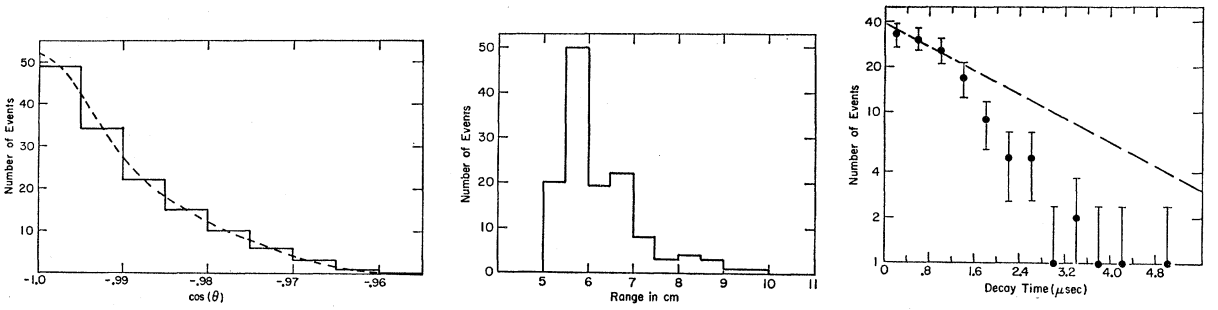

(a) (b) (c)

FIG. 7. Prompt background events from a scattered beam particle. (a) Distribution in $\cos\theta$; (b) distribution in R_e; (c) decay time distribution. The broken line is the muon lifetime fitted to the first 1.2 μsec.

in the target [Fig. 6(d)] or undergoes bremsstrahlung and stops in the target [Fig. 6(e)]. (In such a bremsstrahlung the electron must lose most of its energy so it does not continue on to 2 and give an antipulse, $\bar{2}$.) The gamma ray, which is in the forward direction, is then detected on the gamma side. This gives a prompt coincidence in $E2$, $E1$, T, $\gamma 1$, and $\gamma 2$ with no pulse in 2 or $\bar{\gamma}$, which is just the signature of a real event.

This type of background was eliminated in part by rejecting all events which showed a track from the beam (either a pion or muon) stopping in the $E2$ scintillator or first few range sections at the "end" of the electron track. A total of 133 events of this type were found in the spark chamber and removed from the data. This was about 8% of all the good events. They have the angular and range distributions shown in Figs. 7(a) and 7(b). As the spark chamber was not sensitive to tracks older than about 2 μsec, a certain number still remained in the data. This number was determined by taking the observed events of this type and studying the time distribution of beam particles as determined by the past history display. For particles coming from the beam but missing 2 and T, this display showed a number 1 pulse unaccompanied by a coincident 2 or T. As some beam particles did scatter out of 2 and T, the time of the most recent (1, 2) or (1, 2, T) was taken for these cases. The time plot in Fig. 7(c) shows the decay time of the muon for the first 2 μsec and then falls off more rapidly for times greater than the sensitive time of the spark chamber. The additional background of this kind which could not be rejected by spark chamber tracks was determined graphically. Assuming this background had the time distribution curve of the muon lifetime [broken curve in Fig. 7(c)], the difference between it and the observed distribution must be the number of background events remaining unrejected in the data. There are 80 such events which were then weighted with the angular and range distributions peculiar to this kind of background as found in Figs. 7(a) and 7(b), and then numerically subtracted from the data.

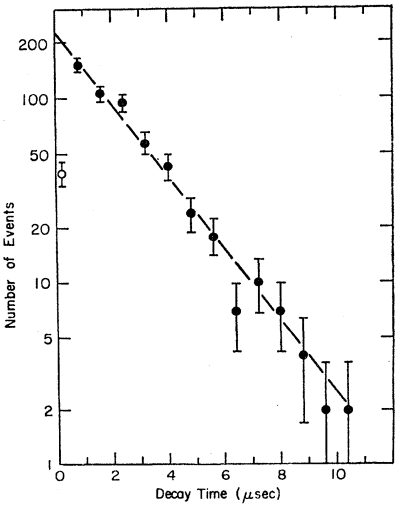

FIG. 8. Decay time distribution of the data. The broken line is the muon lifetime.

The remaining events should not contain any other backgrounds which are independent of the muon lifetime. A check on this estimate, shown in Fig. 8, is obtained from the past history oscilloscope display by plotting the difference in time of arrival of a beam particle (1, 2, T) and its decay (at prompt time on the scope). This indeed shows the muon lifetime with a probable background contamination of less than 5%. The initial point at 0.2 μsec is depressed because the (1, 2, T) gate is not turned on for 0.2 μsec. There are 1533 events in the angular range of $-1 \leq \cos\theta \leq -0.86$. The smaller part of the data which was scanned with large angular acceptance produced 377 events in the range $-0.86 \leq \cos\theta \leq -0.65$.

V. EFFICIENCIES

The efficiencies for detecting the decay $\mu \rightarrow e+\gamma+\nu+\bar{\nu}$ are as follows:

(1) The gate efficiency, i.e., the probability that a muon decays in the target while the gate $(1, 2, T)_G$ is open, was 92.5%. This was determined from the gate delay relative to the (1, 2, T), 0.2 μsec, and the gate length, 11 μsec, with a small correction due to gate

lengthening when two pions entered within 11 μsec of each other.

(2) The efficiency of the electronics for producing a trigger when presented with the proper signature from the counters was 100%, except for the first part of the run where it was 94% due to an error in timing. This decrease in efficiency has been applied as a correction to the number of $(1, 2, T)_G$ during that part of the run.

(3) The probability for a pulse to be visible on all three traces of the 4-beam scope was 100%.

(4) The scanning efficiency was 95%. It was determined by double scanning all of the film and by a third independent scan of some parts of the data.

(5) Since events with 2 electron tracks were rejected, an inefficiency for real events was produced. The probability of a real event not being accompanied by an extra electron was 90% as determined by a scan of the data.

(6) The efficiency for accepting a real event on the basis of the fast timing criteria was 87% because cutoffs were imposed to reduce the number of accidentals.

(7) The loss of efficiency because of accidental pulses, noise, or afterpulsing in $\bar{2}$ and $\bar{\gamma}$ was negligible.

(8) The efficiency for retaining real events after requiring the angle between the gamma ray and its conversion electron be less than 73° was 99%.

(9) The efficiency for the spark chamber to show the tracks of a real event was 100%. This was obtained by the use of multiple gaps at all crucial places so that some spark chamber inefficiency would not cause the rejection of a real event.

The product of all of these efficiencies is

$$\epsilon_0 = 0.925 \times 0.95 \times 0.90 \times 0.87 \times 0.99 = 0.68. \quad (1)$$

All of the efficiencies included in (1) are independent of the energies of the electron and gamma ray and of their angles in the spark chamber.

VI. GAMMA-RAY DETECTION PROBABILITY

As the decay $\mu \rightarrow e+\gamma+\nu+\bar{\nu}$ has a spectrum of energies and angles, it is necessary to fold together the theoretical distributions of the electron and gamma ray with the probabilities that they will be detected in the chamber.

Consider first the probability that the gamma ray is detected. In general, this is a function of only the energy and direction in the chamber

$$P_\gamma(E_\gamma, \cos\phi_\gamma),$$

where ϕ_γ is the angle between the gamma and the normal to the plates. Then the probability T that a gamma ray of energy E_γ is transmitted to a given conversion plate (index i), and the probability that it converts in the plate C, where determined. Since the amount of material traversed by the gamma ray is a function of the angle ϕ_γ, the transmission and conversion probabilities for a given lead plate with index i are

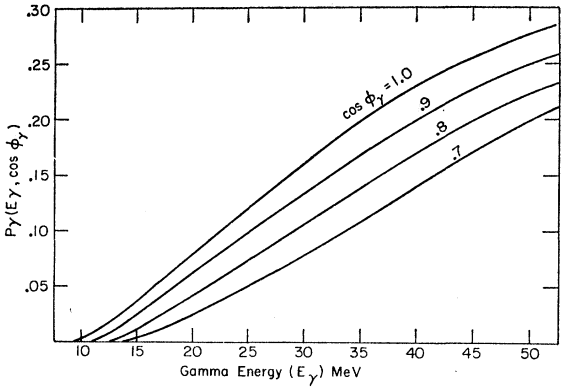

FIG. 9. Plot of the gamma detection probability $P_\gamma(E_\gamma, \cos\phi_\gamma)$ as a function of E_γ for several values of $\cos\phi_\gamma$.

$$T_i(E_\gamma, \cos\phi_\gamma) \quad \text{and} \quad C(E_\gamma, \cos\phi_\gamma). \quad (2)$$

These were determined from the tables of transmissions of gamma rays by Grodstein.[9]

The transmission in lead of electrons produced by monoenergetic gamma rays at 20, 30, and 50 MeV was found by means of Wilson's Monte Carlo calculation[10] and the energy spectrum of electrons emerging from a given thickness of lead was determined. The transmission probabilities in carbon of the electrons of various energies and directions were found from the tables of Leiss, Penner, and Robinson.[11] Combining these results, the probability that an electron produced by a given energy gamma ray penetrates at least half of the $E2$ scintillator is known. This is

$$M(E_\gamma, r, R), \quad (3)$$

and is a function of gamma energy E_γ, range in lead r, and range in carbon R. However, r and R can be approximated by $r_i/\cos\phi_\gamma$ and $R_0/\cos\phi_\gamma$, where r_i and R_0 are the perpendicular ranges in lead and carbon which the conversion electron must traverse in order to be detected. Also, r_i depends on the plate (i) where the conversion takes place. Hence, $M(E_\gamma, r, R)$ becomes

$$M_i(E_\gamma, \cos\phi_\gamma). \quad (4)$$

Combining (2) and (4), the probability that a γ ray converts in one of the lead plates and is detected is

$$P_\gamma(E_\gamma, \cos\phi_\gamma) = \sum_{i=1}^{3} T_i(E_\gamma, \cos\phi_\gamma) C(E_\gamma, \cos\phi_\gamma) \times M_i(E_\gamma, \cos\phi_\gamma). \quad (5)$$

A plot of P_γ is given in Fig. 9 for several values of

[9] G. Grodstein, Natl. Bur. Std. (U. S.) No. 583 (1957).

[10] R. R. Wilson, Phys. Rev. **86**, 261 (1952); and private communication. The actual case histories were used in the efficiency calculation.

[11] J. Leiss, S. Penner, and C. Robinson, Phys. Rev. **107**, 1544 (1957).

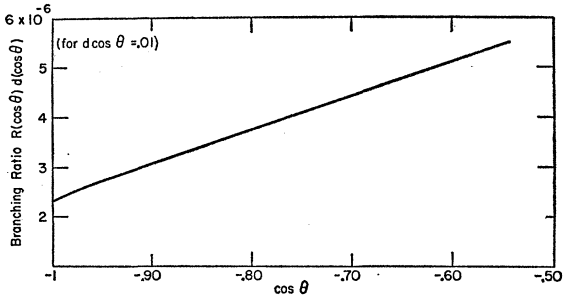

FIG. 10. Angular distribution for inner bremsstrahlung after integrating E_e and E_γ from 12 to 52.8 MeV.

$\cos\phi_\gamma$. The probability is greatest for a gamma ray at 53 MeV and is essentially zero at 12 MeV. The range distribution of the conversion electrons is very broad and shows only a weak dependence on the initial gamma-ray energy. Hence, little information about the gamma-ray spectrum is obtainable and the dependence on gamma-ray energy was removed later by an integration over all possible values of E_γ.

VII. $\mu \rightarrow e+\gamma+\nu+\bar{\nu}$ DETECTION PROBABILITY

The differential branching ratio R of $\mu \rightarrow e+\gamma+\nu+\bar{\nu}/\mu \rightarrow e+\nu+\bar{\nu}$ was calculated using the formulas of Fronsdal and Überall[2] assuming V-A theory. Setting lower limits on the electron and gamma-ray energies of 12 MeV, the plot of the angular distribution for $-1.0 \leq \cos\theta \leq -0.6$ is given in Fig. 10. The electron-energy spectrum for the case, $-1.0 \leq \cos\theta \leq 0.86$, is shown in Fig. 11. For comparison, the Michel spectrum for normal muon decay is shown by the broken curve.

The electron side efficiency calculation is simple as the electron is required only to have a range sufficient to bring it to $ES2$. This efficiency is

$$\begin{aligned} P_e(\cos\phi_e,R_e) &= 1 \quad \text{if} \quad R_e\cos\phi_e > R_2 \\ &= 0 \quad \text{if} \quad R_e\cos\phi_e < R_2, \end{aligned} \tag{6}$$

where R_2 is the range, perpendicular to the plates, from the center of the target to the scintillator E_2, and ϕ_e is the angle of the electron to the perpendicular. R_2 was equivalent to 4.7 cm of graphite.

The predicted differential branching ratio $R(E_e,E_\gamma, \cos\theta)dE_e dE_\gamma d\cos\theta$ was then folded together with the efficiencies of the gamma and the electron side, the various solid-angle factors, and the detection efficiencies ϵ_0 to give the detection probability N per muon decay.

$$\begin{aligned} &N(E_\gamma,E_e, \cos\theta,R_e,\phi_e,\phi_\gamma)d(\cos\phi_e)d\eta d(\cos\theta)dE_\gamma dE_e \\ &= (\epsilon_0)P_\gamma(E_\gamma, \cos\phi_\gamma)P_e(\cos\phi_e,R_e)R(E_e,E_\gamma, \cos\theta) \\ &\quad \times 2\pi d(\cos\phi_e)d\eta d(\cos\theta)dE_\gamma dE_e, \end{aligned} \tag{7}$$

where η is the angle describing a rotation of the electron-gamma plane about the electron direction as an axis. This was simplified by using the geometric relations between the angles ϕ_e, ϕ_γ, η, and θ to eliminate ϕ_γ, and then integrating over the allowed values of $\cos\phi_e$, η, and E_γ.

$$\begin{aligned} &N(\cos\theta,E_e)d(\cos\theta)dE_e \\ &= \epsilon_0\Big[\int\int\int P_\gamma(E_\gamma,\eta, \cos\phi_e, \cos\theta)P_e(\cos\phi_e,R_e) \\ &\quad \times R(E_e,E_\gamma, \cos\theta)d\eta d(\cos\phi_e)dE_\gamma\Big]d(\cos\theta)dE_e. \end{aligned} \tag{8}$$

Equation (8) was then multiplied by the differential probability, $P(E_e,R_e)dR_e$ that an electron with energy E_e will have a true range of R_e to R_e+dR_e cm of carbon. The values of $P(E_e,R_e)dR_e$ were calculated by a Monte Carlo program that allowed for Landau straggling, bremsstrahlung, and annihilation and gave the true rather than the projected range of the positron.[12] After integrating over the energy of the electron E_e, this becomes

$$\begin{aligned} &N(\cos\theta,R_e)d(\cos\theta)dR_e \\ &= \Big[\int N(\cos\theta,E_e,R_e)P(E_e,R_e)dE_e\Big]dR_e d(\cos\theta), \end{aligned} \tag{9}$$

which is the probability that a muon in the target decays by inner bremsstrahlung with an angle θ, is detected in the spark chamber, and has an electron range R_e. The minimum electron energy for detection was about 12 MeV.

The errors in the theoretical calculation result primarily from an uncertainty of about 10% in the energy distributions of the conversion electrons as determined from Wilson's data. An error is introduced by the assumption that the conversion electrons travel in the same direction as the gamma rays which produce them. By taking several values for the angular deviation from colinearity, the over-all error was found to be less than

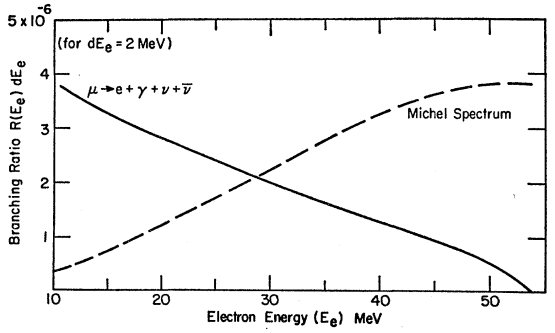

FIG. 11. Electron energy spectrum for $\mu \rightarrow e+\gamma+\nu+\bar{\nu}$ after integrating E_γ from 12 to 52.8 MeV and $\cos\theta$ from -0.86 to -1.0. The broken line is the Michel spectrum normalized to the same area.

[12] S. Parker and C. Rey, in a paper on electron ranges in carbon (to be published). All ranges are in cm of graphite with a density of 1.69 g/cc.

2%. The uncertainty in the various detection efficiencies ϵ_0 is 5%, so the total error is about 15%.

The differential detection probability N in Eq. (9) is now multiplied by the number of pions which stop in the target. This is given by the fraction stopping f, times the number of $(1, 2, T)$. The number f is derived from a calibration run in which the normal $\mu \rightarrow e+\nu+\bar{\nu}$ decay was observed in the chamber. This was done by triggering on $(T, E_1, E_2, \bar{2}, \bar{\gamma})$ gated by $(1, 2, T)$. The number of such decays is given by $P_T = (1, 2, T) f, \epsilon_e, \epsilon_g$. In this equation, $(1, 2, T)$ is the number of beam particles entering the target, f is the fraction which stop, ϵ_e is the calculated efficiency for detecting the decay electron on the electron side of the chamber, and ϵ_g is the gate efficiency. After measuring P_T and $(1, 2, T)$, f was calculated to be 0.61. For the data used in this experiment the number of $(1, 2, T)$ was 1.04×10^{10} and the number of muon decays in the target was 6.43×10^9. The part of the data that was scanned with the larger angular acceptance $(-0.6 \geq \cos\theta \geq -1.0)$ represented 2.34×10^9 $(1, 2, T)$ counts and 1.42×10^9 muon decays in the target.

VIII. RESULTS

The plot of the angular distribution for all data is shown in Fig. 12 and for the section with the larger angle cutoff in Fig. 13. The broken line is the theoretically predicted distribution calculated from Eq. (9). The relative agreement is reasonably good and the absolute agreement is well within the estimated errors. The total number of events in Fig. 12 is 1533 but contains an estimated 4.5% accidental contamination plus an additional 2.5% background from charge exchange. A subtraction gives 1444 ± 41, which is to be compared with a predicted number of 1505 ± 255 for the limits $-1.0 \leq \cos\theta \leq -0.86$. The number of events in the angular range of -0.86 to -0.65 is 377. Subtracting the estimated accidental background of 16 gives 361 real events. The number predicted is 384 ± 57 in this region. The total number of real events is 1805 ± 43 which may be compared with the expected number of 1889 ± 283.

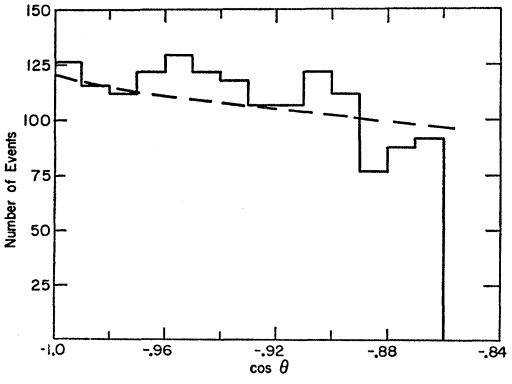

FIG. 12. Angular distribution for data with the range of $-0.86 \geq \cos\theta \geq -1.0$. The broken line is the predicted distribution.

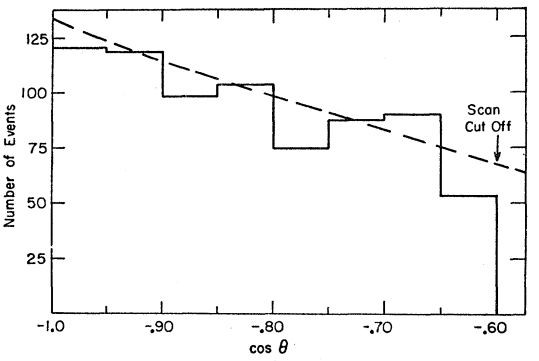

FIG. 13. The angular distribution of the data which has a large acceptance angle $-0.60 \geq \cos\theta \geq -1.0$.

The electron range distributions corresponding to Figs. 12 and 13 are shown in Figs. 14 and 15. These are also in agreement with the theoretically predicted curves (broken lines). The error in the experimental ranges is mostly systematic, since the real range was approximated by adding up a number of short projected ranges obtained in going from one gap to another. The magnitude of this error is estimated to be less than 0.5 cm of graphite. An additional uncertainty occurs because of the thickness of the plate in which the electron stops but these errors tend to average out for all but the first gap.

The dotted curve in Fig. 14 is the range distribution that would be produced in the spark chamber by electrons with the Michel energy spectrum of normal $\mu \rightarrow e+\nu+\bar{\nu}$ decay. The range data of Fig. 14 was smoothed by fitting it with a fourth order curve using the method of least squares. A chi-squared analysis made between the smoothed data and the predicted spectrum of $\mu \rightarrow e+\gamma+\nu+\bar{\nu}$, gives a χ^2 of 2.6 for the ten points from 6 to 16 cm. A similar comparison of the data to the Michel spectrum over the same range gives a poor fit with a χ^2 of 675.

IX. DISCUSSION

Muon decay with inner bremsstrahlung in the region about 180° is adequately described by the V-A theory of weak interactions taken with well-known electromagnetic corrections. Agreement is found for the total rates, the angular distribution and electron-energy spectrum. A calculation by Eckstein and Pratt,[3] shows that the effect of an intermediate vector boson at any point in the energy or angular distributions varies as the inverse square of the boson mass and reaches a maximum of 4% at the kaon mass. The accuracy of this experiment was insufficient to make any statement about the mass of a possible intermediate vector boson.

It is interesting to note that only the absolute magnitude of the weak coupling constant can be measured by observing the total decay rate of the muon. (The correlation between the muon spin and the electron direction does give more information and supports the "V-A"

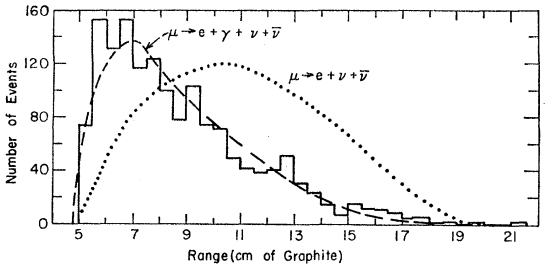

FIG. 14. Range distribution of data corresponding to Fig. 12. The broken curve is the calculated distribution for $\mu \rightarrow e+\gamma+\nu+\bar{\nu}$ and the dotted curve is for $\mu \rightarrow e+\nu+\bar{\nu}$ (Michel spectrum) normalized to the same number of events.

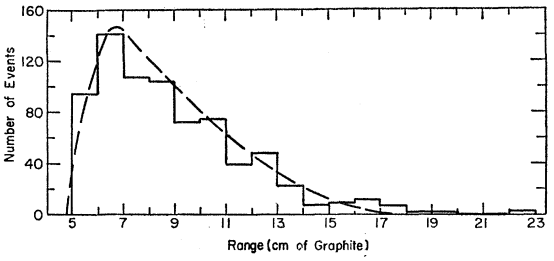

FIG. 15. Range distribution of the data corresponding to Fig. 13. The broken line is predicted.

theory.[13]) In the most general form, the weak interaction constant is a combination of five couplings[2]: scalar(C_s), pseudoscalar(C_p), vector(C_v), axial vector (C_a), and tensor(C_t). If g_s, g_v ang g_t are defined as follows: $g_s=|C_s|^2+|C_p|^2$, $g_v=|C_v|^2+|C_a|^2$, and $g_t=|C_t|^2$, then the total rate of muon decay is proportional to $(g_s+4g_v+6g_t)$.

In inner bremsstrahlung, the different couplings produce somewhat different angular correlations and energy spectra but such effects are too small to be detectable in the present experiment. This can be seen from the way the inner bremsstrahlung depends on these couplings. The differential rate R is given by

$$R(E_e,E_\gamma,\theta)=g_sN_S+g_vN_V+g_tN_T,$$

where the N_i are functions of E_e, E_γ, and θ. N_T is almost identical to N_V in form, but is larger ($N_T \cong 2N_V$). Therefore, one cannot distinguish between the g_v and g_t contributions. N_S is about 1/20 as large as N_T but does have a somewhat different dependence on E_e, E_γ, and θ. The Michel parameter ρ is given in these terms by $(1-\frac{4}{3}\rho)=g_s-2g_t$, hence if $\rho \cong 0.75$,[13] then $g_s \cong 2g_t$. Substituting these relations in R gives

$$R \simeq 2g_tN_S+g_vN_V+g_t2N_V=N_V[g_v+2g_t(1+\Delta)], \quad (10)$$

where $\Delta \equiv N_S/N_V \simeq 0.05$. For the values of E_e, E_γ, and θ used in this experiment, Δ varies only by ± 0.01. In (10) the difference is a very small effect and so a separation of the contributions from g_s and either g_t or g_v cannot be made. Hence the data is consistent with the predictions of V-A theory but does not eliminate other coupling schemes.

In this decay the electromagnetic features predominate and the specific form of the weak interaction has little effect. However, the inner bremsstrahlung of the muon is the only case of a weak particle decay entirely free of strong interactions. Hence, the electromagnetic corrections can be unambiguously applied and tested. The data are in accord with theory and thus substantiate the predictions given by electromagnetic corrections to the weak decay process. The experimental technique is also applicable to some extent to the investigation of radiative effects in other particles which exhibit leptonic decays.

ACKNOWLEDGMENTS

The author wishes to express his sincere thanks to Professor Herbert L. Anderson for suggesting this experiment and for his guidance and sponsorship of this research. I am also indebted to Dr. Sherwood Parker for his interest in this work and for his valuable assistance. I am grateful also to C. S. Johnson, R. Gabriel, L. Lavoie, and W. Stanula for their aid in the experiment, and to E. Mayer, M. Raymond, and H. Rabinovitz for their valuable help in the analysis of the data.

[13] R. J. Plano, Phys. Rev. **119**, 1400 (1960).